Non adiabatic electron behavior through a supercritical perpendicular collisionless shock: Impact of the shock front turbulence

Philippe Savoini, Bertrand Lembège

Non adiabatic electron behavior through a supercritical perpendicular collisionless shock: Impact of the shock front turbulence

P. Savoini[1] and B. Lembege[2]

Received 23 February 2010; revised 7 June 2010; accepted 1 July 2010; published 6 November 2010.

[1] Adiabatic and nonadiabatic electrons transmitted through a supercritical perpendicular shock wave are analyzed with the help of test particle simulations based on field components issued from $2-D$ full-particle simulation. A previous analysis (Savoini et al., 2005) based on $1-D$ shock profile, including mainly a ramp (no apparent foot) and defined at a fixed time, has identified three distinct electron populations: adiabatic, *overadiabatic*, and *underadiabatic*, respectively, identified by $\mu_{ds}/\mu_{us} \approx 1$, >1 and <1, where μ_{us} and μ_{ds} are the magnetic momenta in the upstream and downstream regions. Presently, this study is extended by investigating the impact of the time evolution of $2-D$ shock front dynamics on these three populations. Analysis of individual time particle trajectories is performed and completed by statistics based on the use of different upstream velocity distributions (spherical shell of radius v_{shell} and a Maxwellian with thermal velocity v_{the}). In all statistics, the three electron populations are clearly recovered. Two types of shock front nonstationarity are analyzed. First, the impact of the nonstationarity along the shock normal (due to the front self-reformation only) strongly depends on the values of v_{shell} or v_{the}. For low values, the percentages of adiabatic and overadiabatic electrons are almost comparable but become anticorrelated under the filtering impact of the self-reformation; the percentage of the underadiabatic population remains almost unchanged. In contrast, for large values, this impact becomes negligible and the adiabatic population alone becomes dominant. Second, when $2-D$ nonstationarity effects along the shock front (moving rippling) are fully included, all three populations are strongly diffused, leading to a larger heating; the overadiabatic population becomes largely dominant (and even larger than the adiabatic one) and mainly contributes to the energy spectrum.

Citation: Savoini, P., and B. Lembege (2010), Non adiabatic electron behavior through a supercritical perpendicular collisionless shock: Impact of the shock front turbulence, *J. Geophys. Res.*, *115*, A11103, doi:10.1029/2010JA015381.

1. Introduction

[2] Breakdown of electron adiabaticity through a collisionless shock has been investigated in previous works within two complementary approaches: a statistical approach and an individual approach.

1.1. Statistical Approach

[3] This approach is based on local electron distribution function $f_e(\vec{v})$ measured from the upstream to the downstream region. Observations [*Montgomery et al.*, 1970; *Feldman et al.*, 1982; *Feldman*, 1985; *Scudder et al.*, 1986a, 1986b, 1986c; *Schwarz et al.*, 1988] have evidenced a parallel velocity distribution which becomes flat-topped with a power law tail (for a review, see *Scudder* [1995]). This particular shape of $f_e(\vec{v})$ within the shock front can be explained by the interaction of electrons with the macroscopic electric field at the ramp and has been fully recovered by $2-D$ full particle-in-cell (PIC) electromagnetic simulations [*Savoini and Lembège*, 1994] and by a theoretical Vlasov-Liouville model [*Hull et al.*, 1998, 2001]. All of these studies have emphasized the importance of the space-charge electric field built up at the shock ramp, which is responsible for the energy gain of this population when penetrating the downstream region. Moreover, the perpendicular heating is mainly controlled by the magnetic field and the majority of transmitted electrons suffer an adiabatic compression [*Feldman*, 1985; *Krauss-Varban*, 1994; *Scudder et al.*, 1986a; *Scudder*, 1995; *Hull et al.*, 2001].

[4] Nevertheless, the adiabaticity may be broken through a supercritical shock even for moderate Mach number [*Scudder et al.*, 1986c; *Schwarz et al.*, 1988]. Different mechanisms may be invoked. The most evident concerns the small-scale turbulence present at the shock front, which scatters efficiently the energetic electrons as shown numerically [*Krauss-Varban*, 1994; *Krauss-Varban et al.*, 1995] and experimentally [*Scudder et al.*, 1986c]. Another possibility does not

[1]LPP, Ecole polytechnique, UPMC, Palaiseau, France.
[2]LATMOS-UVSQ-CNRS-IPSL, Guyancourt, France.

0148-0227/10/2010JA015381

require turbulence and is based on the narrowness of the shock ramp [*Newbury and Russell*, 1996; *Newbury et al.*, 1998; *Walker et al.*, 1999a], so that electrons do not follow the magnetic field variations and the magnetic moment is not conserved anymore.

1.2. Individual Approach

[5] Conversely, the individual approach follows electron trajectories, which allows one to investigate their divergence in the velocity space (i.e., using Lyapounov coefficient γ). As infered by *Cole* [1976] and shown by *Balikhin et al.* [1993], *Gedalin et al.* [1995a, 1995b, 1995c], *Ball and Galloway* [1998], *Balikhin et al.* [1998], and *Ball and Melrose* [2001], the electric field gradient ($\vec{\nabla}E$) can be responsible for a noticeable percentage of demagnetized electrons within the ramp, which appears to be a good candidate for nonadiabatic heating. These conclusions have been recovered by using self-consistent full particle simulations [*Lembège et al.*, 2003].

[6] Test particle simulations [*Savoini et al.*, 2005] allow one to investigate the electron trajectories through a stationary supercritical and perpendicular collisionless shock. This numerical approach is quite appropriate to control the initial particle locations both in real and velocity space (phase space dependence analysis). To suppress any contribution of oblique propagation effects, this analysis has been restricted to a strictly perpendicular shock ($\theta_{Bn} = 90°$ where θ_{Bn} is the angle between the shock normal and the upstream magnetic field). Surprisingly, even for this simple case, two distinct nonadiabatic populations have been identified in addition to adiabatic particles (defined with the ratio $\mu_{ds}/\mu_{us} \approx 1$ where μ is the magnetic momentum, and "ds" and "us" hold, respectively, for downstream and upstream values of μ averaged over a few gyroperiods after and before the shock front crossing: first, an *overadiabatic* population characterized by $\mu_{ds}/\mu_{us} > 1$, and second, an *underadiabatic* population, not predicted by the theory, and characterized by $\mu_{ds}/\mu_{us} < 1$. Any possible drift effect has been eliminated in the estimate of μ by substracting the perpendicular mean bulk velocity component calculated over each gyromotion of the particle. A simplified theoretical model has been proposed to classify these two populations according to their injection angle θ_{inj}, defined between the local gyrating velocity vector (in the reference frame of the particle) and the shock normal at the time the electron hits the shock front. *Underadiabatic* electrons are characterized by small injection angles $\theta_{inj} \leq 90°$, whereas *overadiabatic* particles have higher injection angles $\theta_{inj} > 90°$.

[7] Nevertheless, these test particle results have been obtained for a uniform (along the shock front) and stationary shock (fixed profile at a given time) issued from 2-D full particle simulations. However, it is largely evidenced from experimental measurements [*Galeev et al.*, 1988; *Krasnoselskikh et al.*, 1991; *Balikhin et al.*, 1997; *Walker et al.*, 1999b] and from simulations [*Biskamp and Welter*, 1972; *Forslund et al.*, 1984; *Lembège and Dawson*, 1987; *Winske and Quest*, 1988; *Lembège and Savoini*, 1992] that the shock front is intrinsically nonstationary, even for moderate but still supercritical Mach numbers. One source of nonstationarity along the shock normal invoked to account for some in situ experimental data [*Horbury et al.*, 2001] is the so-called self-reformation of the shock front observed in full particle-in-cell (PIC) simulations [*Lembège and Dawson*, 1987; *Lembège and Savoini*, 1992; *Scholer et al.*, 2003]. During this process, the amplitude of the foot (due to the accumulation of reflected ions) increases in time until reaching a value comparable to that of the ramp at earlier times, starts reflecting new incoming ions, and the process cyclically repeats. As a consequence, the shock front varies quasi-periodically over a typical ion gyro-period scale ($T_{reformation} \approx \tau_{ci,ramp}$ where $\tau_{ci,ramp}$ is the mean local ion gyro-period in the ramp and averaged over one reformation). During this process, the ramp and the foot are alternatively well separated (steepy ramp with a thickness of a few electron inertia lengths) or mixed (smoother ramp with a larger thickness). Consequently, one expects the final downstream electron behavior to differ depending on the local field gradients at the time they hit the shock front and the resulting downstream electron heating to be time-dependent for a given high Mach number shock.

[8] The purpose of the present paper is to address this issue by extending our previous test particle simulations [*Savoini et al.*, 2005] to different shock profiles issued from self-consistent 2-D PIC simulations including both nonstationarity and nonuniformity of the shock front. Section 2 contains a brief description of the $2-D$ full-particle simulations used to analyze the supercritical collisionless shock. Section 3 examines the time behavior of electron trajectories for three typical shock profiles selected within one self-reformation cycle and the statistics deduced from an initial shell electron distribution. Section 4 presents statistics based on different upstream shell distributions for three different shock profiles (fixed time each) and for a continously time-varying shock. Section 5 summarizes statistics obtained for a Maxwellian distribution where nonstationary and nonuniformity effects are analyzed separately. Conclusions are presented in section 6.

2. Numerical Conditions

[9] Self-consistent field components of a strictly perpendicular shock are obtained from a $2-\frac{1}{2}D$ fully electromagnetic, relativistic PIC code using standard finite-size particle techniques whose details have been given in *Lembège and Savoini* [1992] and *Savoini and Lembège* [1994]. The use of a full-particle code is necessary to obtain all nonstationary E and B field components measured at different times, in particular the cross-shock electric field which is expected to play a key role in the dynamics of transmitted electrons.

[10] Basic properties of the numerical code are summarized as follows. Nonperiodic conditions are applied along x-direction within the simulation box, and periodic conditions are used along the y-direction. The plasma simulation box lengths are $\widetilde{L}_x = 6144$ and $\widetilde{L}_y = 256$, which represents 102 and 4.3 inertial ion length ($\widetilde{c}/\widetilde{\omega}_{pi}$), respectively. Initial plasma conditions (i.e., upstream region) are summarized as follows (all physical parameters are normalized to dimensionless quantities identified by a tilde "~"): light velocity $\widetilde{c} = 3$, electron thermal velocity in each direction $\widetilde{v}_{the,x,y,z} = 0.3$, temperature ratio between ion and electron population $T_i/T_e = 1.58$.

[11] The magnetostatic $\widetilde{B}_o$ field (0, 0, 1.5) is along z axis. The Alfven velocity is $\widetilde{v}_A = 0.075$. The shock propagates in

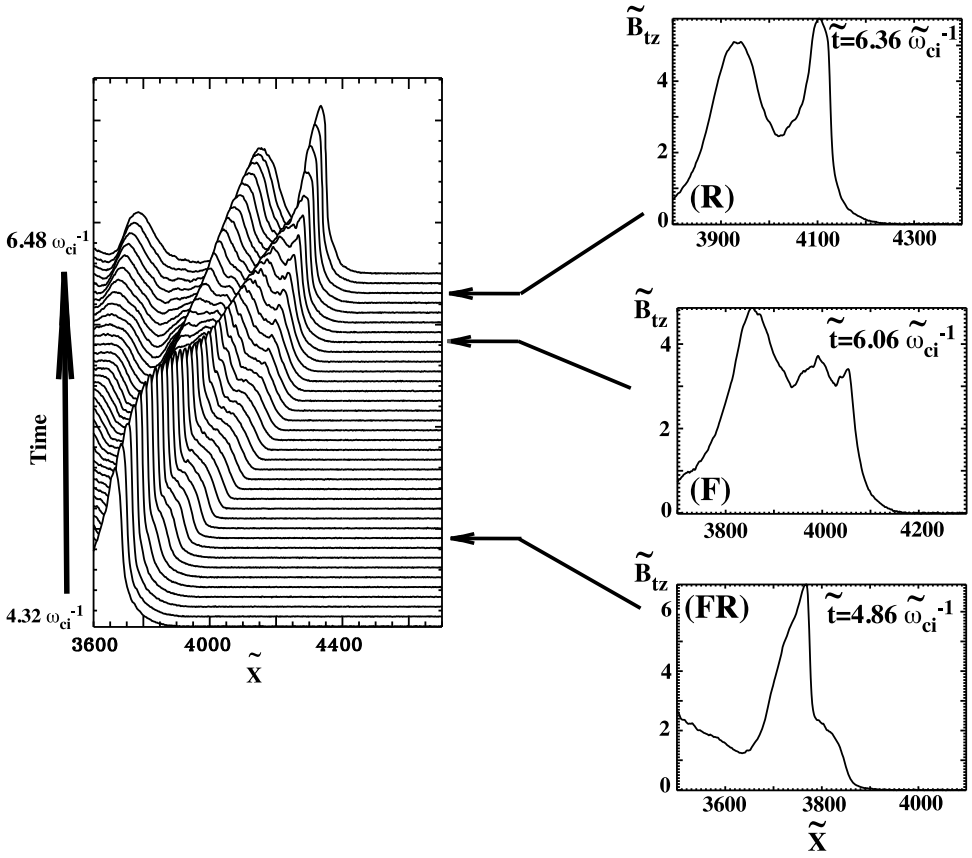

Figure 1. Left: time-stackplots of y-averaged $\widetilde{B}_{tz}$ component within a whole reformation cycle ($4.32\widetilde{\omega}_{ci}^{-1} \leq \widetilde{t} \leq 6.48\widetilde{\omega}_{ci}^{-1}$). Right: enlarged views of the main $\widetilde{B}_{tz}$ component around the shock front at three different selected times, where the front profile is respectively dominated by the ramp (**R**), the foot (**F**) and both foot and ramp (**FR**). These profiles show the different characteristic profiles that test electrons can meet at the shock front. The propagation angle is $\theta_{Bn} = 90°$.

a supercritical regime (M_A = 5.14), characterized by a noticeable density of reflected ions.

[12] A detailed study of the electron dynamic and trajectories requires the use of a high mass ratio approaching realistic value as much as possible. Nevertheless, at present, $2-D$ self-consistent full-particle simulations are still difficult to perform for a realistic mass ratio $M_i/m_e = 1836$. Only $1-D$ shock simulations manage to include such realistic mass ratio [*Liewer et al.*, 1991; *Scholer et al.*, 2003]. As a compromise, a mass ratio $M_i/m_e = 400$ is used in this paper, which is high enough to separate the dynamics of electrons and ions and to obtain more realistic space-charge effects at the ramp than for lower mass ratio used in previous studies. To analyze in detail the impact of the shock front nonstationarity on the directly transmitted electrons, a three-stage analysis has been developed:

[13] 1. First, only nonstationary effects along the shock normal (x-direction) are included. All effects of nonstationarity [*Lembège and Savoini*, 1992; *Scholer et al.*, 2003] and nonuniformity [*Forslund et al.*, 1984; *Savoini and Lembège*, 1994] along the y-direction are suppressed by y-averaging all field components. Figure 1 shows characteristic magnetic shock profiles selected at three different times within one self-reformation cycle ($4.32\widetilde{\omega}_{ci}^{-1} \leq \widetilde{t} \leq 6.48\widetilde{\omega}_{ci}^{-1}$): a common "foot-ramp" profile (FR) with a "small" magnetic foot ($\widetilde{t} = 4.86\widetilde{\omega}_{ci}^{-1}$), a "foot-dominated" profile (F) where the foot amplitude is higher than the half of the total magnetic jump between upstream and downstream region ($\widetilde{t} = 6.06\widetilde{\omega}_{ci}^{-1}$), and a "ramp-dominated" profile (R) where no foot is "apparent" ($\widetilde{t} = 6.36\widetilde{\omega}_{ci}^{-1}$). $\widetilde{\omega}_{ci}$ is the upstream ion cyclotron frequency. Herein the self-reformation cyclic period is $\widetilde{T}_{reformation} = 0.32\widetilde{\tau}_{ci}$, where $\widetilde{\tau}_{ci}$ is the upstream ion cyclotron period.

[14] (2) Second, the same test electrons are analyzed as they cross the profiles of self-consistent $2-D$ shock, where both nonstationarity and nonuniformity are fully included (no y-averaging). The shock profiles defined at the same three times are used.

[15] (3) Third, the self-consistent time evolution of the shock wave is included to study the impact of the full temporal variation of the shock front.

3. Individual Particle Trajectories Analysis

[16] In initial conditions of all runs, test particles are released at rest (in the solar wind frame) at a distance $\widetilde{d}_{upstream} = 220\widetilde{\rho}_{ce}$ upstream from the shock front (where $\widetilde{\rho}_{ce}$ is the upstream electron gyroradius), and are distributed over a shell in $3-D$ velocity space (section 4) and as a Maxwellian

(section 5). The shock front is forced to move with a velocity $\widetilde{v}_{shock} = 0.38$ equal to the shock velocity measured in the $2 - D$ full particle simulation. Similar to the numerical method used by *Savoini et al.* [2005], the different transmitted electron populations are identified by the variation of their individual magnetic moment $\mu = mv_{\perp}^2/2B$ between upstream and downstream regions. This moment is computed in the inertial particle frame where $v_{\perp}$ holds for the gyrating velocity only where all velocity drifts (e.g., $\vec{E} \times \vec{B}$, $\vec{B} \times \vec{\nabla} B$) have been eliminated.

[17] Figure 2 shows the time evolution of the ratio μ/μ_{us} as electrons cross the shock front for the three characteristic profiles defined in Figure 1 (the velocity components are defined with respect to the local magnetic field $\vec{B}$). Different parts of the shock profiles (ramp, foot) are seen by each electron during time ranges which are defined between dashed lines (Figures 1e, 1j, and 1o) and are reported correspondingly in the other parts of Figure 1. The **R** profile (no apparent foot) is used as a reference, since it has already been studied in detail in a previous paper [*Savoini et al.*, 2005]. All test electrons hit the shock front at the same time, and the main results for this particular **R** profile are summarized as follows:

[18] 1. *Adiabatic electron* (Figure 1l), hereafter called particle $part_a$. After the front crossing, the ratio μ/μ_{us} fluctuates around ≈1.2 in the downstream region.

[19] 2. *Overadiabatic* electron (Figure 1m), hereafter called particle $part_b$. The ratio μ/μ_{us} rises up to its maximum value ($\mu/\mu_{us} \approx 10$) and fluctuates around 7 further downstream.

[20] 3. *Underadiabatic* electron (Figure 1n), hereafter called particle $part_c$. As the electron penetrates the shock ramp, the ratio μ/μ_{us} suffers a drastic drop down from ≈1 to 0.15 during a short time range $\Delta\widetilde{t} \approx 10\widetilde{\omega}_{ce}^{-1}$, where $\widetilde{\omega}_{ce}$ is the local electron gyrofrequency, i.e., within the first half of the ramp, and remains roughly constant as the particle penetrates further the shock front and the downstream region. This last class can be identified in terms of particle injection angle [*Savoini et al.*, 2005].

[21] A comparison of results obtained for these **R**, **F**, and **RF** profiles stresses the strong impact of the varying field gradients seen by the transmitted electrons when crossing the shock front, although the same electron is considered in the three cases. The main changes can be summarized as follows.

[22] 1. *Particle* $part_a$: This electron has an adiabatic behavior in both the **F** and **R** profiles. However, it has an *overadiabatic* behavior for the **FR** profile ($\mu_{ds}/\mu_{us} \approx 3$).

[23] 2. *Particle* $part_b$: In contrast to the **R** profile, the same electron becomes *underadiabatic* with the **FR** profile. This difference is explained in terms of local injection angle θ_{inj} and with the help of our simple theoretical model [*Savoini et al.*, 2005]. This θ_{inj} dependence is even more emphasized in the **F** profile, where the electron shows opposite variations of μ when crossing, respectively, the "old" ramp and the "new" ramp, where the "new" ramp is building up at the leading edge of the increasing foot. As a result, these variations compensate each other so that the final ratio $\mu_{ds}/\mu_{us} \approx 1$ and the particle may be considered as adiabatic.

[24] 3. *Particle* $part_c$: The electron exhibits quite different behavior with respect to the **R** profile. Both **FR** and **F** profiles lead to a final ratio $\mu_{ds}/\mu_{us} > 1$, and the electron is *overadiabatic*, which means that the foot, even of small amplitude, has a strong influence.

[25] All these results mean that the final state of transmitted electrons does not depend only on their features within the first half of the ramp when the shock is not reduced to a ramp as in the **R** profile. Other criteria need to be defined when the nonstationarity of the shock front is included. In addition, the present analysis of individual particle trajectories reveals them not to be powerful enough to reach general statements on the transmitted electrons, and/or to predict the final downstream behavior of a given particle. Instead of analyzing particles further case-by-case, we have chosen to focus on statistical analysis to prepare a possible comparison with experimental data.

[26] As an extension of our previous paper [*Savoini et al.*, 2005], we consider successively two different types of initial upstream electron distribution: mono-/multiple shell distributions (section 4) and a Maxwellian distribution (section 5).

4. Statistical Analysis for Mono-/Multiple Shell Distributions

[27] In this first step, 580 electrons are distributed over a velocity sphere of radius $\widetilde{v}_{shell} = 0.26$ (Figure 3a), so that only the phase angles differ from one particle to the other. In the upstream region, the x-direction of the shock propagation corresponds to the $\perp_2$ axis (Figure 3b). This shell distribution has been built in such a way that at any given perpendicular velocity component (i.e. over a circle of $\widetilde{v}_{\perp}$ radius), the number of electrons remains identical. Then, this shell distribution has the advantage of relative simplicity but has the drawback of oversampling high $\widetilde{v}_{\parallel}$ electron contribution (with small $\widetilde{v}_{\perp}$ component) as compared with very low $\widetilde{v}_{\parallel}$ electron contribution (with high $\widetilde{v}_{\perp}$ component).

4.1. Impact of the Time-Varying Shock Front for a Fixed Shell Radius (Monoshell)

[28] As evidenced in Figure 1, the shock front continuously evolves through **R**-**FR**-**F** profiles within one cyclic self-reformation. Then several test simulations using the same shell distribution have been repeated to analyze the transmitted electrons through about 36 different shock profiles previously stored on each $0.01\widetilde{\omega}_{ci}^{-1}$ time step within the time range $\widetilde{t} = 4.32\widetilde{\omega}_{ci}^{-1}$ to $\widetilde{t} = 6.48\widetilde{\omega}_{ci}^{-1}$ (Figure 1) covering one self-reformation. Following the classification of section 3, we have plotted in Figure 4 the relative percentage of adiabatic (thick line), *overadiabatic* (thin line) and *underadiabatic* electrons (dashed line) obtained in the downstream region versus time. For reference, the three shock profiles used in section 3 have been reported. Each simulation is stopped after typically $3.2\widetilde{\omega}_{ci}^{-1}$ when all injected electrons are transmitted far enough in the downstream region.

[29] Two characteristic time ranges can be identified from Figure 4. First, a long time range T_1 ($3450(4.31\widetilde{\omega}_{ci}^{-1}) \leq \widetilde{t} \leq 4490(5.61\widetilde{\omega}_{ci}^{-1})$) is mainly characterized by a drastic variation (decrease and increase) of adiabatic electrons percentage (from 80% to 40% as time increases) simultaneously anticorrelated to a strong variation of the *overadiabatic* population (from 10% to 45%).The striking feature is that both variations compensate each other. In contrast, the third population (*underadiabatic*) oscillates around 10% without clear correlation with both the adiabatic and the *overadiabatic*

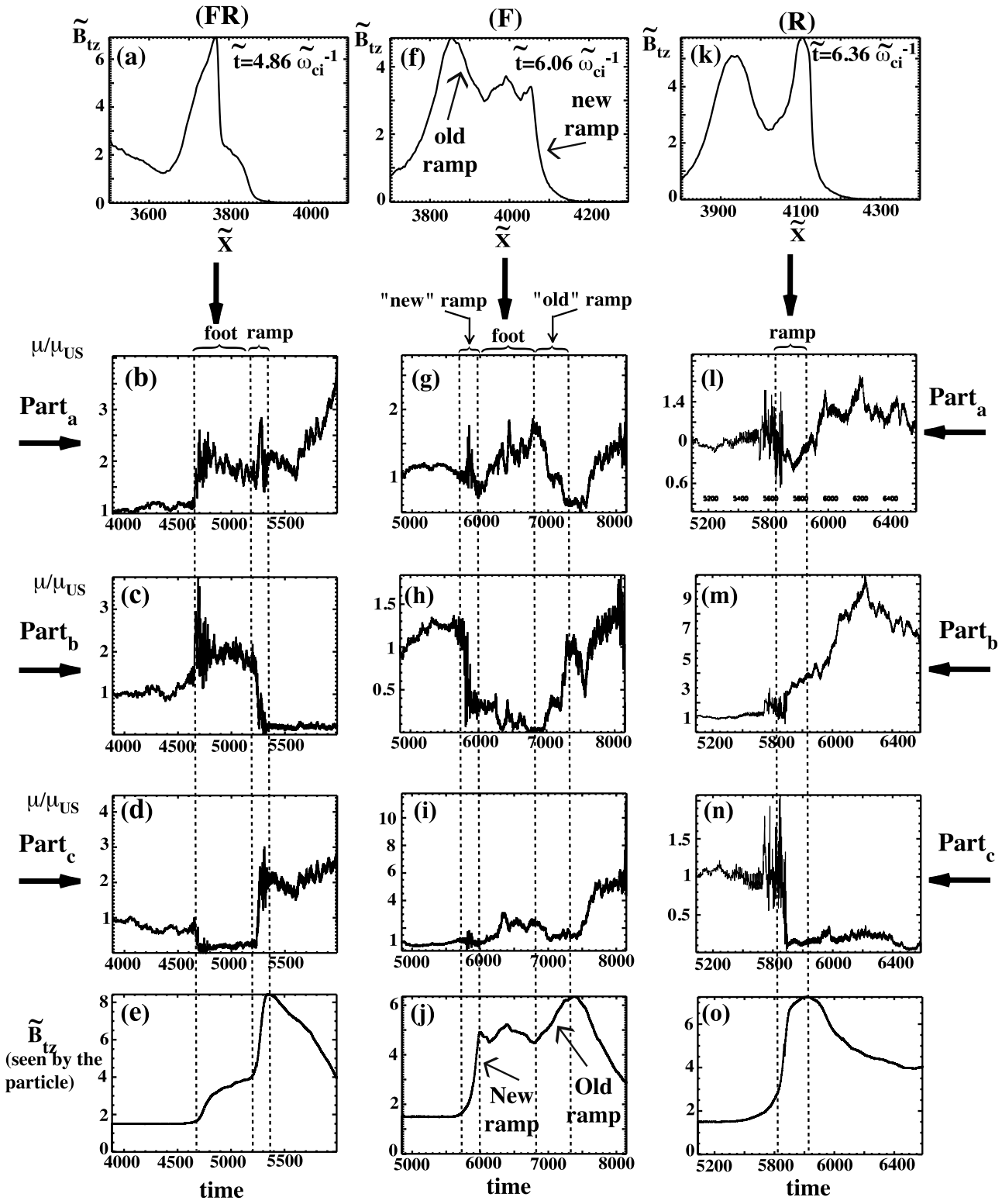

Figure 2. Time histories of the magnetic momenta ratio μ/μ_{us} (where $\mu = mv_{\perp}^2/2B$, and B is the local magnetic field seen by the particle) of three selected electrons as they cross the three shock profiles **FR**, **F** and **R** selected in Figure 1. Subscript "us" means "upstream". These three particles are among 580 electrons distributed over a spherical shell with a radius $\widetilde{v}_{shell} = 0.26$. For reference, Figures 2e, 2j, and 2o show the $\widetilde{B}_{tz}$ component seen by the particles.

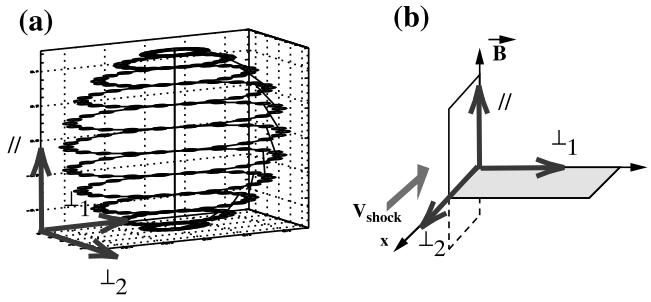

Figure 3. (a) Spherical shell of 580 electrons (test particles) initially released at an upstream distance $\widetilde{x} = 220\widetilde{\rho}_{ce}$ from the moving supercritical shock front. (b) Sketch of the reference set where coordinates are chosen in the shock frame at time t = 0. The upstream magnetostatic field $\vec{B}_o$ is along z axis (outside the simulation plane).

populations. Moreover, the T_1 period can be associated with a progressive buildup of the foot (**R**-**FR** type shock profile) as evidenced in the middle part of Figure 4. Second, another shorter time interval T_2 ($4490(5.61\widetilde{\omega}_{ci}^{-1}) \le \widetilde{t} \le 5030(6.29\widetilde{\omega}_{ci}^{-1})$) is characterized by a high percentage of adiabatic electrons (about 80%), by only few nonadiabatic (i.e. *over*- and *underadiabatic*) electrons and by the progressive steepening of the foot into a new ramp (**F** profiles). To understand this behavior, we have reported (top) the maximum amplitude of the magnetic field gradient measured at the ramp versus time (the ramp defined during T_1 is replaced by the "new" ramp during T_2). Also reported (middle) are the locations of the leading edge of the shock front (thin line), of the ramp (dashed line), and of the overshoot (thick line). During interval T_1, the ramp thickness (defined between dashed and thick lines) is minimum ($\approx 4\widetilde{c}/\widetilde{\omega}_{pe}$), and the magnetic field gradient reaches its maximum value (≈ -0.6). In contrast, during interval T_2, the ramp thickness becomes much larger while the magnetic field gradient reaches its minimum value (≈ -0.06).

[30] Then, when varying in time, the shock front appears to have an important filtering effect on transmitted electrons. The percentage variation during interval T_1 is not surprising (see *Savoini et al.* [2005]). Indeed, the reinforced local gradient of the electric field (associated with the very thin ramp during the shock front self-reformation) is quite appropriate to extract some electrons from the adiabatic "soup" and to force these electrons to reach an overadiabatic level. The value of this gradient at the ramp is the strongest (0.044) for a **FR** shock profile (Table 1) as observed within interval T_1. The opposite variation applies within interval T_2. Then the variation of the magnetic field gradient (top of Figure 4) reveals itself to be a good indicator to account for the variation of the *overadiabatic* electron percentage and its anticorrelation with adiabatic electrons percentage (to compare top and bottom).

[31] In contrast, within both time intervals T_1 and T_2, the main percentage of *underadiabatic* electrons only evidences fluctuations (even high) around 10% but without correlation with the other populations. Such behavior is in agreement with the paper of *Savoini et al.* [2005], which shows that their existence mainly depends on the local injection angle θ_{inj} measured at the shock front hitting time and not on the magnetic field gradient itself. Section 3 has evidenced that a given electron belonging to a given class (for a fixed shock profile) changes its class as the shock front varies. Present statistics indicate that the shock front variation redistributes electrons in such a way that the percentage of *underadiabatic* population is almost unchanged for $v_{shell} = 0.26$.

4.2. Impact of the Time-Varying Shock Front for Different Fixed Shell Radii v_{shell} (Multiple Shell)

[32] The previous section has provided results for a fixed radius (v_{shell}) of the shell distribution, but no information on the impact of a varying shell radius on adiabaticity breakdown for different shock profiles. For reasons of simplicity, we follow a procedure similar to that used in Figure 4 for different values of $\widetilde{v}_{shell}$. We have scanned the whole upstream distribution function in velocity space by injecting for each selected shock profile a series of shells with different radii from 0.01 to 1.3 with a variation $\delta\widetilde{v}_{shell} = 0.05$, but only three of them are presented on Figure 5 for clarity. We observe that as $\widetilde{v}_{shell}$ increases, two velocity domains can be defined, depending approximately on the thermal velocity: (1) for $\widetilde{v}_{shell} \le \widetilde{v}_{the,\perp}$ (where the upstream perpendicular thermal velocity $\widetilde{v}_{the,\perp} \approx 0.37$), lots of transmitted electrons are nonadiabatic. However, for (2) $\widetilde{v}_{shell} \ge \widetilde{v}_{the,\perp}$, nearly all electrons become adiabatic. These results confirm quantitatively that the breakdown of adiabaticity takes place mainly for low gyrating velocity (independently of their phase or injection angle), whatever the shock profile is, i.e., the impact of the nonstationarity is relatively weak.

[33] This evolution is clearly shown in Figures 5a, 5b, and 5c. For $\widetilde{v}_{shell} < \widetilde{v}_{the,\perp}$ ($\widetilde{v}_{shell} = 0.06$, Figure 5a), the same behavior is observed as in Figure 4 ($\widetilde{v}_{shell} = 0.26$), but with higher percentages of nonadiabatic electrons. In particular, the *overadiabatic* electrons are dominant (and anticorrelated to adiabatic ones) within the part of time range T_1 where the magnetic field gradient is maximum (≈ -0.6 within $3600(4.5\widetilde{\omega}_{ci}^{-1}) \le \widetilde{t} \le 3800(4.75\widetilde{\omega}_{ci}^{-1})$) and stays almost comparable within interval T_2. In a first approach, the percentage of *underadiabatic* electrons is almost independent to the shock front profile and only fluctuates around an averaged value of $\approx$17%. In contrast, for $\widetilde{v}_{shell} \ge \widetilde{v}_{the,\perp}$ ($\widetilde{v}_{shell} =$ 0.4 and 0.51 of Figures 5b and 5c, respectively), approximately 90% of the transmitted electrons are adiabatic. Only a relatively weak (anticorrelated) variation between *underadiabatic* as in Figure 5b (*overadiabatic* as in Figure 5c) and adiabatic electron percentage is observed within the whole self-reformation cycle ($T_1 + T_2$) and reaches a maximum around time $\widetilde{t} = 4250(5.31\widetilde{\omega}_{ci}^{-1})$. In summary, the nonstationarity has a stronger impact within a certain v_{shell} range below $\widetilde{v}_{the,\perp}$ ($0.06 \le \widetilde{v}_{shell} \le 0.26$ in the present case), within which *overadiabatic* and adiabatic electrons reach comparable percentage values. One striking feature is that the percentage of *underadiabatic* electrons globally decreases drastically as $\widetilde{v}_{shell}$ increases. Although this population shows important variations in time for $\widetilde{v}_{shell} \le 0.4$, no clear correlation of these variations with the shock nonstationarity has been observed.

[34] One can conclude that the evidence of the *underadiabatic* population (not performed experimentally until now) is preferentially expected for very low $\widetilde{v}_{shell}$ value. On the other hand, these results can account for some experimental observations obtained by *Schwarz et al.* [1988]

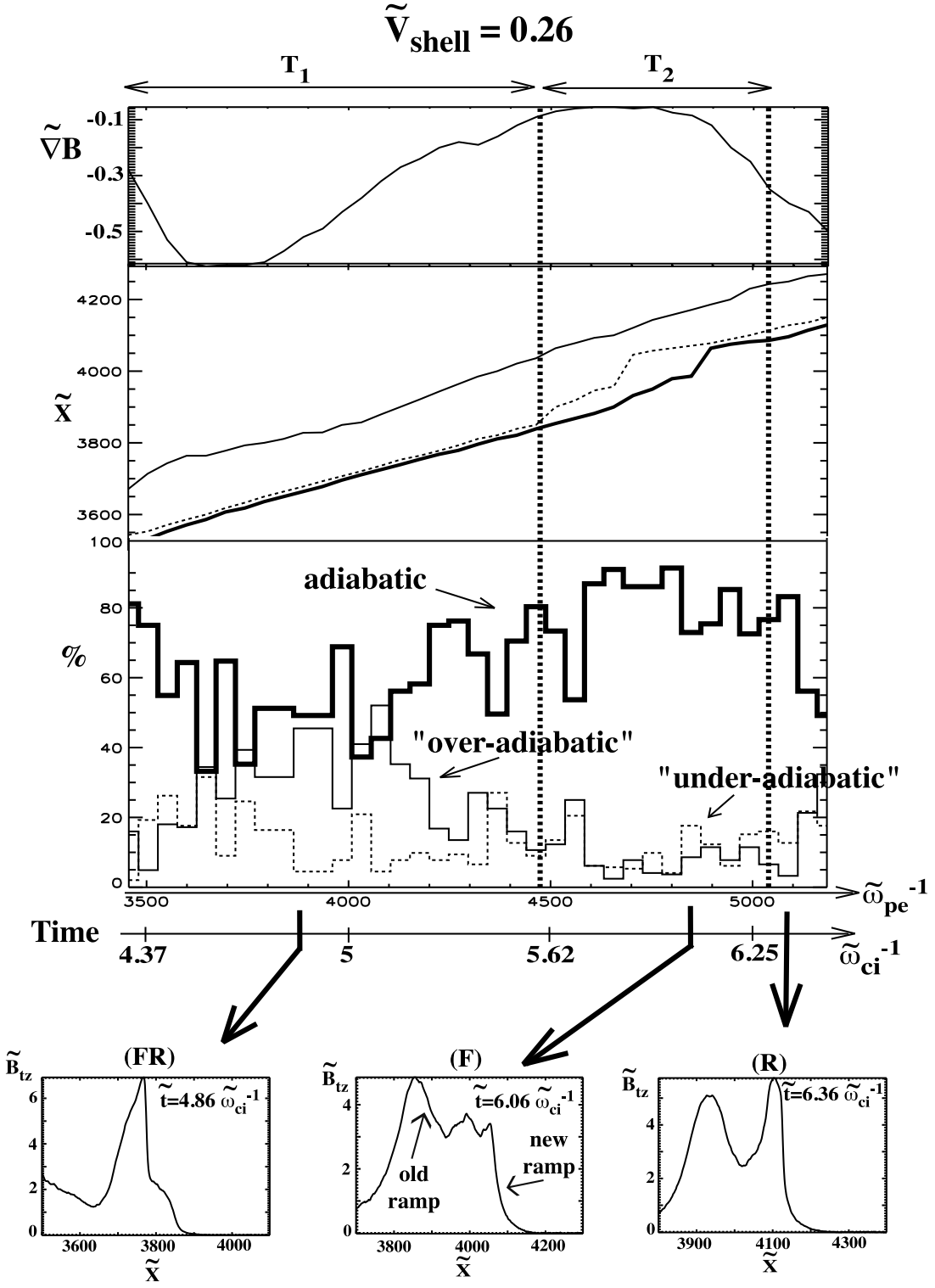

Figure 4. Percentage of adiabatic ($\mu_{ds}/\mu_{us} \approx 1$, thick line), *underadiabatic* ($\mu_{ds}/\mu_{us} < 1$, dotted line) and *overadiabatic* ($\mu_{ds}/\mu_{us} > 1$, thin line) electrons versus time during a self-reformation cycle of the shock front as defined in Figure 1 (left). For each given time, a new run is performed with the same set of shell particles ($\tilde{v}_{shell} = 0.26$) released at the same upstream position from the shock front. The top shows the maximum amplitude of the magnetic field gradient measured along x at the ramp. In the middle are reported the x-locations of the leading edge of the shock front (thin line), of the leading edge of the ramp (dashed line) and of the overshoot (thick line). The three selected shock profiles (Figure 1, right) have been reported for reference. The average downstream value μ_{ds} is computed over many gyrations after the electron penetrates the overshoot region.

Table 1. Values of the Electric Field Gradient Measured in the Different Parts (Foot and Ramp) of the Shock Front for the Different Selected Profiles, **R**, **F** and **FR**, Respectively[a]

	$\frac{dE}{d_{ramp}}$	$\frac{dE}{d_{foot}}$
R	0.007	X
F	0.0014	0.0027
FR	0.044	0.0018

[a]For the **F** type profile, the gradient is measured at the "new" ramp. For the **R** type profile, "X" means that no measurement is possible since no noticeable foot can be identified.

where *overadiabatic* heating is not observed for shocks with relatively high upstream electron thermal velocity.

5. Statistical Analysis for a Maxwellian Distribution

[35] Our simple model of a discrete shell in the velocity space has the advantage of relative simplicity but has some limitations: (1) the injected electron velocities are strictly limited to the $0 \leq \widetilde{v} \leq \widetilde{v}_{shell}$ range with a uniform velocity distribution in $\widetilde{v}_{\perp}$; and (2) particle angular diffusion is allowed for a given $\widetilde{v}_{shell}$ radius, but no diffusion in velocity amplitude (i.e., equivalent to diffusion between different $\widetilde{v}_{shell}$ radii). These features are far from a real distribution of the solar wind. To resolve these questions, a Maxwellian distribution is used instead of a shell to describe initially the test particles. This requires much more particles to satisfy statistical constraints. Figure 6 displays results obtained for a Maxwellian distribution ($f(\widetilde{v}_{\|}), f(\widetilde{v}_{\perp 1}), f(\widetilde{v}_{\perp 2})$) with a thermal velocity $\widetilde{v}_{the} = 0.26$ released at the same distance from the shock front ($\widetilde{d}_{upsteam} = 220\widetilde{\rho}_{ce}$) for the same three shock profiles **R**, **FR** and **F** used in previous sections. Moreover, one takes again advantage of the fact that test particles have no feedback on the fields to follow less particles ($N_{el} = 1500$) to save computation time. As a result, Maxwellian functions are more noisy than in full PIC simulations, but statistics are strong enough for the present purpose.

5.1. Fixed Shock Front Profiles

[36] For each profile (Figure 6), we have superimposed on the same image the total upstream distribution (thick line) defined at initial time, and the upstream distribution of the adiabatic (dotted line), of the *underadiabatic* (thin line) and of the *overadiabatic* (gray shadow) populations according to results obtained in the downstream region. Such plots allow us to determine precisely which part of the upstream distribution, downstream nonadiabatic/adiabatic electrons are coming from. For all cases, relative percentage values are reported in Table 2.

[37] First, let us consider the **R** profile for its relative simplicity. We retrieve that the main part of the distribution exhibits an adiabatic behavior. The percentage of adiabatic particles for the Maxwellian distribution (94%) is even larger than that found for the shell model (86%) for $\widetilde{v}_{shell} = 0.26$ (Table 2). This difference can be explained by the fact that while all the individual velocities are limited to the radius value $\widetilde{v}_{shell}$ in the shell distribution, a larger number of energetic electrons with $\widetilde{v} > \widetilde{v}_{the}$ exist in a Maxwellian. Consequently, more adiabatic particles are expected according to the results of section 4. Moreover, Figure 6 confirms that nonadiabatic particles are mainly issued from the core of the perpendicular upstream distribution function ($-0.2 \leq \widetilde{v}_{\perp} \leq 0.2$). In addition, the parallel distribution $f(\widetilde{v}_{\|})$ is almost uniform within the velocity range $-0.6 \leq \widetilde{v}_{\|} \leq 0.6$ for both *over-* and *underadiabatic* electrons. This indicates that the **R** profile acts as a filter which produces nonadiabatic electrons among particles having small perpendicular (gyrating) velocity for any corresponding parallel velocity.

[38] Second, the buildup of the foot (**FR** profile) has three main impacts. (1) the percentage of *underadiabatic* electrons strongly increases as simultaneously the percentage of adiabatic ones decreases (summarized in Table 2). This behavior is even more in evidence in Figures 7b and 7c, which show an increase of the *underadiabatic* population between the times $5\omega_{ci}^{-1} \leq T \leq 5.62\omega_{ci}^{-1}$ when the foot builds up in front of the shock wave and at the same time no clear variation of the *overadiabatic* population. (2) The percentage of *overadiabatic* electrons remains very weak. (3) Nonadiabatic electrons are not issued from the core of the upstream distribution anymore. Results (1) and (2) seem in apparent contradiction with those obtained for a shell distribution (section 4) but are a consequence of the particle diffusion (in velocity amplitude) not accessible in a shell distribution. Indeed, suprathermal particles with $\widetilde{v}_{\perp} > \widetilde{v}_{the}$ in a Maxwellian distribution are in favor of adiabaticity. In spherical shell, particles do have the same total velocity $v_{total} = \sqrt{v_{\|}^2 + v_{\perp}^2} = v_{shell}$, while these are randomly distributed for a Maxwellian. Then, no direct correlation can be established for a Maxwellian between parallel and perpendicular velocity components.

[39] Third, as the foot continues to increase (**F** profile) and becomes dominant, the percentage of adiabatic electrons increases again at the expense of the *underadiabatic* electrons whose percentage decreases (Table 2). Let us be reminded that electrons have to cross successive regions where field gradients are quite different, including a "new" and an "old" ramp. Consequently, the local conditions in terms of both field gradients and of injection angle are drastically changing during the shock crossing. Then all combinations of electron behaviors are possible and compensate each other in such a way that they are statistically irrelevant, filling out the whole perpendicular distribution functions. However, two interesting features appear: (1) During the transition from **F** to **R** profiles, a steepening of the "new" ramp takes place and acts to select progressively nonadiabatic electrons, not from the whole Maxwellian, but from the core only; and (2) moreover, during the transition from **R** to **FR** profiles, the increasing foot has a filtering effect equivalent to transferring electrons from the adiabatic to the *underadiabatic* population. Furthermore, this filtering process can be invoked because for all profiles, the percentage of *overadiabatic* electrons is relatively weak and remains almost unchanged whatever the shock profile is.

[40] For a further investigation, we have performed in the same format as Figure 5 simulations with a Maxwellian distribution for three different thermal velocities $\widetilde{v}_{the} = 0.06$, 0.26 and 0.51. Results reported in Figures 7a–7c present some similarities with those obtained for a shell distribution. Results of Figure 7a ($\widetilde{v}_{the} = 0.06$) and Figure 5a ($\widetilde{v}_{shell} = 0.06$) are quite similar. The increase (decrease) of *overadiabatic* (adiabatic) electrons is very time-localized (anticorrelation). Let us note that for the present case where $\widetilde{v}_{the} = 0.06$, most

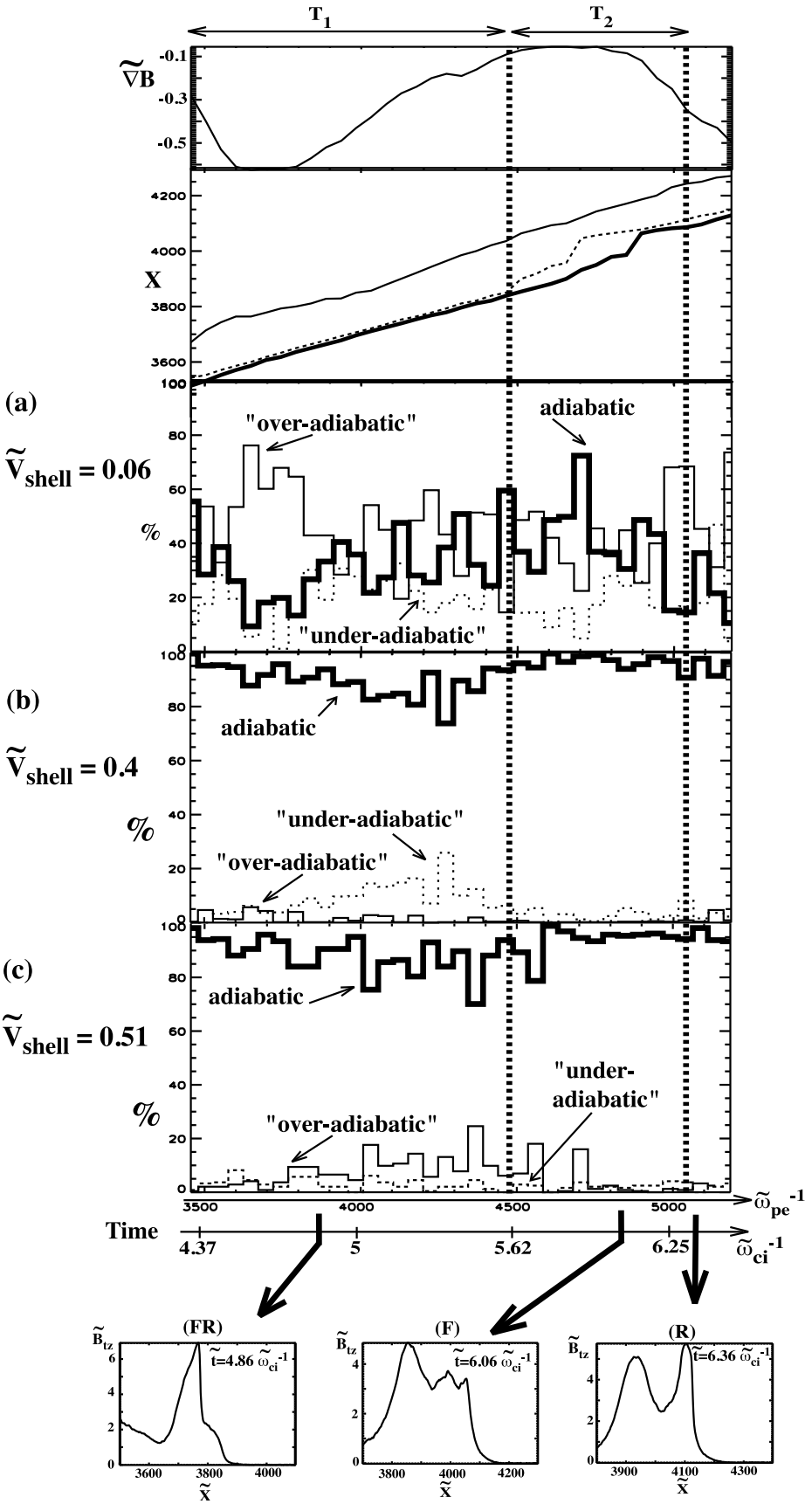

Figure 5. Similar to Figure 4 for larger radius of the upstream shell distribution $\tilde{v}_{shell}$ = 0.06 (a), 0.4 (b), and 0.51 (c).

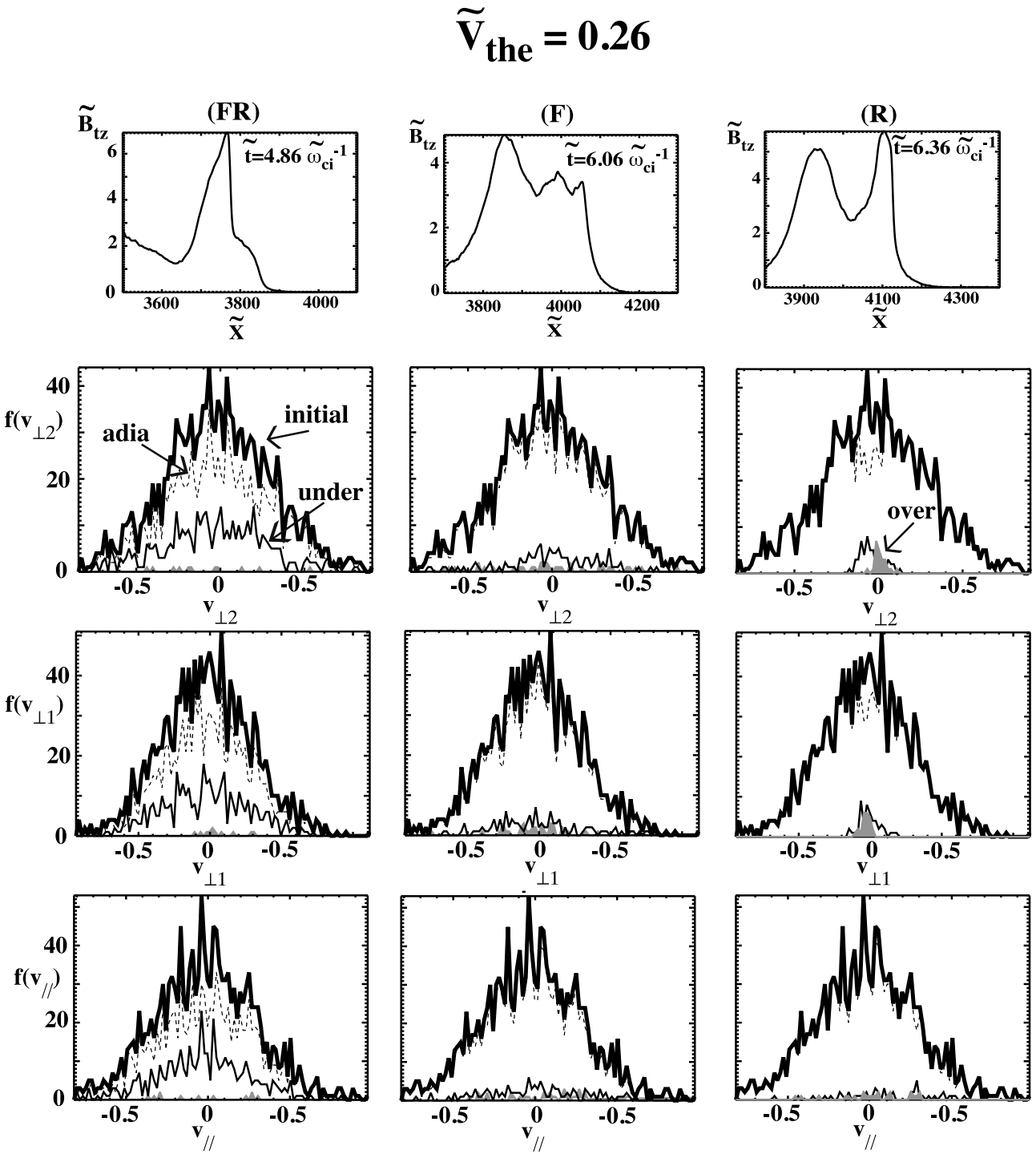

Figure 6. Electron distribution functions obtained for an upstream Maxwellian distribution ($\tilde{v}_{the} = 0.26$) of test particles ($N_e = 1500$) released at an upstream distance $\tilde{x} = 220\tilde{\rho}_{ce}$ from the shock front. Results are obtained for the three shock profiles defined in Figure 1, which are reported at the top. Total distribution is represented by a thick line. *Underadiabatic* (thin line), *overadiabatic* (gray shadow), and adiabatic (dashed line) distributions are superimposed on each plot for comparison and are represented according to the original location they occupy in the upstream distribution.

electrons verify the condition $\tilde{v}_{\perp} < \tilde{v}_{the}$, and a noticeable percentage of nonadiabatic electrons is evidenced in good agreement with conclusions obtained from a shell distribution. For higher $\tilde{v}_{the}$, the direct comparison between $\tilde{v}_{the} = 0.26$ (Figure 7b) and $\tilde{v}_{shell} = 0.26$ (Figure 4) is difficult as explained in the previous section due to the limitation of the shell model, and we have to take into account a $\tilde{v}_{shell} = 0.4$ (Figure 5b) to cover approximately the velocity distribution of the Maxwellian with $\tilde{v}_{the} = 0.26$. The two Figures 5b and 7b show similarities concerning the variation between non-

Table 2. Percentage of *Adiabatic*, *Underadiabatic* and *Overadiabatic* Electrons (Measured With Respect to the Total Transmitted Electrons) Through the Three Selected Shock Profiles, **R**, **F** and **FR**, Respectively[a]

%	*Adiabatic*	*Underadiabatic*	*Overadiabatic*
	$\widetilde{v}_{the}$ = 0.06/0.26/0.51($\widetilde{v}_{shell}$ = 0.26)		
R	26/94/98 (86)	30/4/1 (4)	44/2/1 (10)
F	40/85/94 (84)	23/11/5 (10)	37/4/1 (6)
FR	45/84/95 (89)	25/12/4 (7)	30/4/1 (4)

[a]For each profile, the upstream Maxwellian distribution is defined with $\widetilde{v}_{the}$ = 0.06, 0.26 and 0.51 respectively (Figures 7a–7b), and for a shell distribution with $\widetilde{v}_{shell}$ = 0.26 in bracket (Figure 4).

adiabatic and adiabatic electron percentages within the whole self-reformation cycle. Adiabatic electrons are again dominant. For even higher $\widetilde{v}_{the}$ (0.51 as in Figure 7c), adiabatic (nonadiabatic) electrons become largely dominant (poor) and the shock nonstationarity has a weak impact on each population. Only a weak anticorrelation is observed between adiabatic and *underadiabatic* electrons with a maximum around time $\widetilde{t}$ = 4250 ($5.31\omega_{ci}^{-1}$).

[41] In summary, two relevant criteria defining the behavior of directly transmitted electrons whatever is the upstream distribution (shell/Maxwellian) may be stressed out: (1) the condition $\widetilde{v}_{\perp} < \widetilde{v}_{the}$ is necessary to observe downstream nonadiabatic electrons, and (2) in the absence of a noticeable foot (**R** profile), the condition $\theta_{inj} \leq 90°$ needs to be satisfied for identifying *underadiabatic* particles among the nonadiabatic ones. Additional statistics (not shown here) allow us to conclude that, only for the **R** type shock profile, nonadiabatic electrons are issued from a specific part (core) of the upstream distribution.

5.2. Impact of the Full Two-Dimensional Nonstationary and Nonuniformity of the Shock Front

[42] At this stage, it is important to remind that all previous results have been obtained for shock profiles (1) selected at certain times, and (2) where nonuniformity and nonstationarity effects along the shock front (front rippling) have been suppressed by y-averaging. Obviously, the time-dependent field variations are expected to modify the electron dynamic, and it is important to analyze a fully time-varying shock profile. With this purpose in mind, we have performed a $2-D$ PIC simulation identical to that described in section 2 and save all field components of the shock on each $0.05\widetilde{\tau}_{ce}$ time step (where $\widetilde{\tau}_{ce}$ is the upstream electron gyroperiod), to retain all electron scale fluctuations. These shock profiles stored over one self-reformation cycle ($5.16\widetilde{\omega}_{ci}^{-1} \leq \widetilde{t} \leq 7.0\widetilde{\omega}_{ci}^{-1}$) are introduced in a test particle simulation where a Maxwellian velocity distribution $f(v)$ similar to that used in section 5 ($\widetilde{v}_{the}$ = 0.26) is released. The following procedure allows us to clearly identify the impact of the self-consistent rippling of the shock front on electron dynamics.

[43] In a first step, we perform a spatial y-averaging for each profile to obtain a uniform shock (no front rippling), but where nonstationarity due to the shock front reformation along x axis is still included with a much higher time resolution than in previous sections. As a reference, a time stackplot of the magnetic field component is reported in Figure 8a (slightly different from that of Figure 1). We have indicated with arrows the time $T_{in} = 5.40\widetilde{\omega}_{ci}^{-1}$ when the upstream Maxwellian distribution hits the shock front (approaching **FR** type profile) and the time $T_{out} = 6.24\widetilde{\omega}_{ci}^{-1}$ when it reaches the downstream region (leaving the shock front). During the shock crossing, transmitted electrons see a varying shock profile corresponding to a continuous time transition between **FR**-**F**-**R** profiles defined in Figure 1.

[44] Results are summarized as follows (Figures 8b and 8c). (1) Adiabatic electrons are again dominant (as expected from previous sections for a value v_{the} = 0.26). (2) The percentages of *over-* and *underadiabatic* populations are comparable. (3) Each population is individually heated through the shock and is widely spreading within a whole Maxwellian. However, the results of Figures 8b and 8c differ from those of Figure 6 in the sense that the continuously time-varying front contributes to an increase the percentage of *overadiabatic* electrons at the expense of adiabatic ones (percentages of electrons for each population are respectively reported in Table 3).

[45] In a second step, we have performed test particle simulations on the basis of the same shock profiles but without y-averaging, i.e., where shock front rippling is fully included. In present case, the rippling has been identified as due to lower hybrid frequency waves propagating along the shock front and excited by cross-field current instabilities as in *Lembège and Savoini* [1992]. A detailed analysis of waves contributing to the shock rippling is presently under active investigation and results will be presented in a further paper. The impact of the shock front rippling on the transmitted electron dynamics is important and can be summarized as follows (compare Figures 8e–8g with Figures 8b–8d). (1) The percentage of *overadiabatic* electrons drastically increases and becomes even larger than that of adiabatic ones, which strongly decreases (Table 3). (2) Comparatively, the *underadiabatic* electrons are less affected but nevertheless suffer some diffusion. (3) The spread of each distribution strongly increases (strong individual heating). (4) *Overadiabatic* electrons are coming from the whole upstream distribution and not only from the core. Feature (1) was expected in the sense that the shock rippling contributes to particle diffusion in time and space and consequently to the adiabaticity breakdown. In contrast, feature (2) was unexpected and stresses that *underadiabatic* electrons are mainly controlled by the macroscopic field components at the front along the shock normal, and less by any nonstationarity/inhomogeneity along the shock front. Corresponding energy spectra (Figures 8d and 8g) confirm the above results and, in particular, that the front rippling makes the *overadiabatic* population dominant. The important diffusion suffered by each population leads to an important change in the slope of each spectrum. The power law coefficient strongly differs from $p \approx -4.7$ for the first case (without front rippling) to $p \approx -0.6$ for the second one (with front rippling). The difference between both without/with front rippling cases illustrates quantitatively the impact of the cross-field current instabilities (front rippling) on the dynamic of all electron populations, in particular the *overadiabatic* electrons, which are strongly heated.

[46] Moreover, the important difference observed in the behavior of *overadiabatic* and *underadiabatic* populations indicates that their respective origin strongly differs. One is very localized in time and in space (injection angle depen-

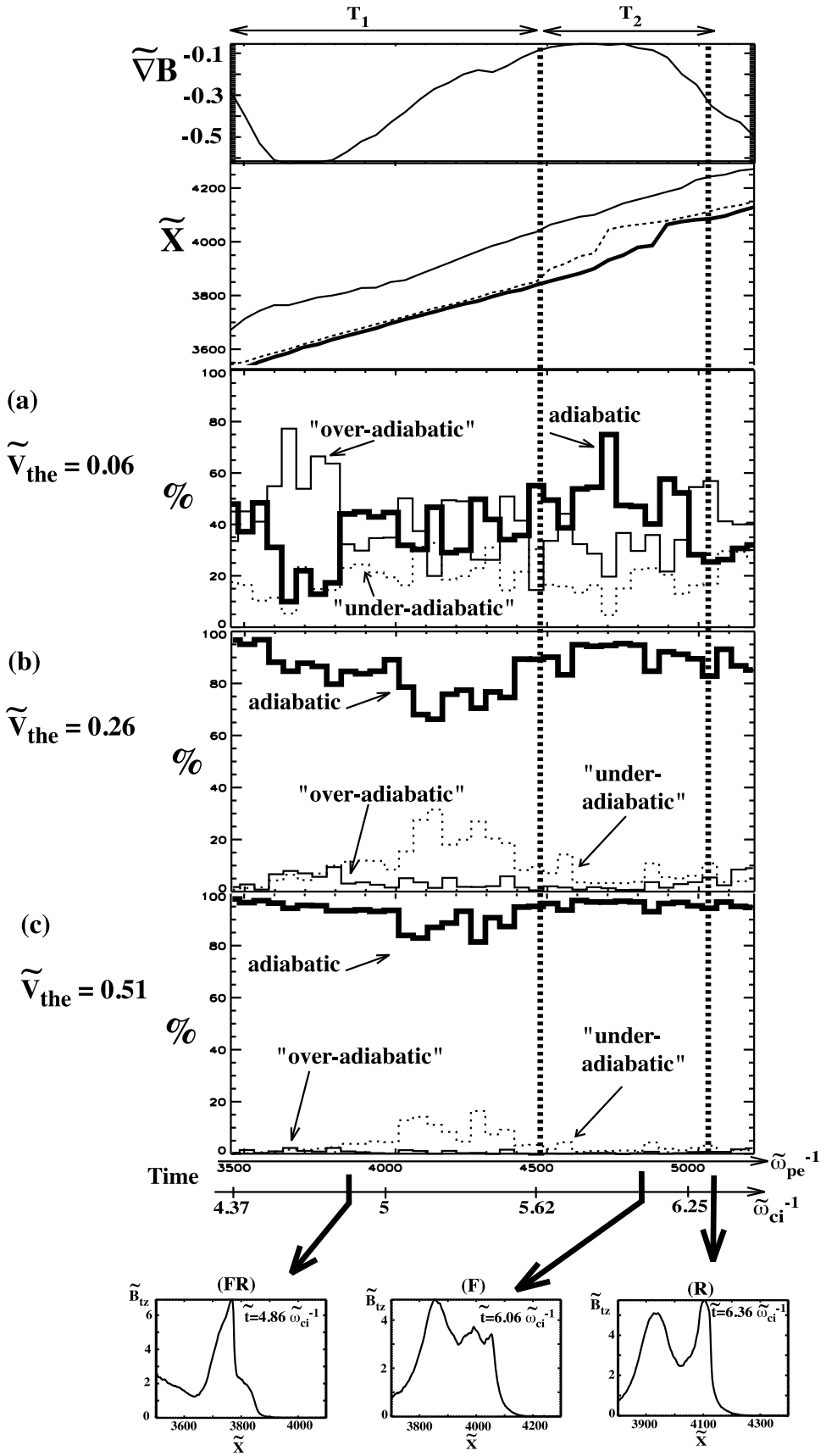

Figure 7. Similar to Figures 4 and 5 for an upstream Maxwellian distribution with $\tilde{v}_{the} = 0.06$ (a), 0.26 (b), and 0.51 (c).

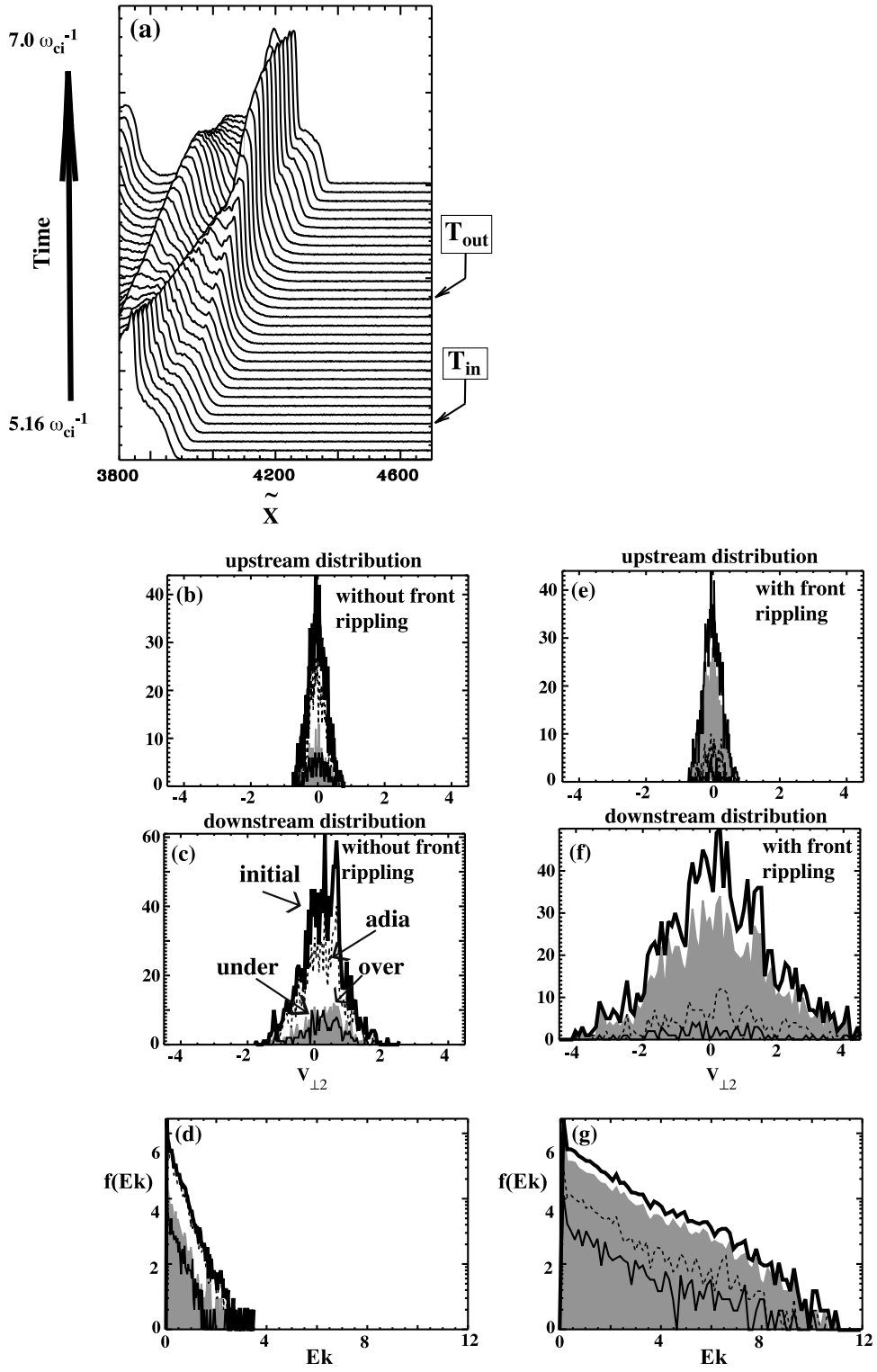

Figure 8. Results obtained for a nonstationary $2-D$ shock front continuously evolving within a time range covering a full self-reformation cycle. Upstream electrons hit and leave the shock front downstream at time T_{in} and T_{out} respectively (Figure 8a). Two cases are reported: Figures 8b–8d (resp. Figures 8e–8g) as the shock front rippling is excluded (y-average) or included (no y-average). After being identified in the downstream region, the different populations are reported according to their original location they occupy in the upstream distribution (Figures 8b and 8e) as in Figure 6. Figures 8c and 8d (Figures 8f and 8g) represent the final distribution (downstream region) and the corresponding energy spectra (semilog graph) for shock fronts without (with) ripples.

Table 3. Percentage of the Three Classes of Transmitted Electrons Populations for an Upstream Maxwellian Distribution ($\widetilde{v}_{the} = 0.26$) Crossing a 2-D Fully Self-consistent (self reforming) Shock Front Without and With Front Rippling (Figure 8)

%	*Adiabatic*	*Underadiabatic*	*Overadiabatic*
without rippling	79	8	13
with rippling	30	10	60

dance for the *underadiabatic*) and is not strongly affected by the field fluctuations. The other one applies on a much longer time/space range, leading to a higher sensitivity to these same field fluctuations.

[47] A comparison (not shown here) between the two simulations (with and without front rippling) evidences that less than 30% of the *overadiabatic* population comes from the macroscopic electric field gradient at the front. What is left (70%) corresponds to perpendicular heating associated with the front rippling.

6. Discussion and Conclusions

[48] We have investigated the adiabatic/nonadiabatic behavior of the transmitted electrons through a supercritical perpendicular shock by means of test particle simulation where field components are issued from self-consistent $2-D$ full-particle simulations. The present analysis is an extension of a previous study [*Savoini et al.*, 2005] restricted to a fixed $1-D$ shock front defined at a given time and characterized by a ramp profile mainly (no noticeable foot), to a $2-D$ shock front profile varying in time and space during self-reformation. This has allowed us to emphasize the key role of some criteria used to separate adiabatic/nonadiabatic electron populations and to identify more precisely both nonadiabatic populations. The resulting electron distribution measured downstream appears as a mixture of these three classes of heated electrons. Present statistics based successively on mono-/multiple spherical shell distributions and on different Maxwellian distributions show the following.

[49] 1. The three types of transmitted electron population persist independently of the concerned initial distribution and on the shock front nonstationarity/nonuniformity. These appear as a permanent feature in supercritical perpendicular shock wave, even for a moderate Mach number regime.

[50] 2. The relative percentage of the three populations strongly varies, depending on the upstream radius value $\widetilde{v}_{shell}$ (for shell distribution) and on the thermal velocity $\widetilde{v}_{the}$ (for a Maxwellian distribution). In particular, for very weak upstream $\widetilde{v}_{the}$ (or $\widetilde{v}_{shell}$ value), the *overadiabatic* population dominates. In contrast, adiabatic population is largely dominant for warmer upstream population, and the percentage of both nonadiabatic populations becomes weak. This result is in a good agreement with experimental results obtained by *Schwarz et al.* [1988] stating that the number of nonadiabatic transmitted electrons drastically decreases as the upstream temperature increases. These results persist whatever the shock profile and/or the upstream population is (shell or Maxwellian).

[51] 3. The impact of the nonstationarity along x (different shock profiles) on these percentages strongly depends on the values $\widetilde{v}_{shell}$ or $\widetilde{v}_{vthe}$. For the purpose of simplicity, let us increase progressively the upstream temperature from low values. For relatively cold distribution (very small $\widetilde{v}_{shell}$ or $\widetilde{v}_{the}$), nonstationarity effects have a negligible impact on each population. For slightly larger $\widetilde{v}_{shell}$ or $\widetilde{v}_{the}$ (0.06, for instance) such that the percentages of adiabatic and *overadiabatic* electron become comparable, nonstationary effects have a filtering impact leading to an anticorrelated variation in their relative percentages independently of the upstream distribution. However, as the distribution becomes warmer ($\widetilde{v}_{shell}$ or $\widetilde{v}_{the} = 0.26$), this anticorrelation becomes smoother, but some features vary according to the upstream distribution of concern. As the distribution becomes even much warmer ($\widetilde{v}_{shell}$ or $\widetilde{v}_{the} = 0.51$), the impact of the shock front nonstationarity is weaker on each population. In summary, this impact is the strongest within a certain range (herein $0.06 < \widetilde{v}_{shell} \leq 0.26$ for a shell, and $\widetilde{v}_{the} \ll 0.26$ for a Maxwellian). Within these ranges, an anticorrelation is only observed between adiabatic and *overadiabatic* populations, while the *underadiabatic* population remains insensitive to any shock turbulence.

[52] 4. The impact of the "full" nonstationarity along x only: some differences occur between statistics obtained at a given time T_{in} (fixed shock profile only) and those performed when "fully" including the nonstationary effects starting at this same time T_{in}. The nonstationarity of the shock front redistributes electrons between the different populations in such a way that the percentage of adiabatic electrons decreases, at the advantage of *overadiabatic* ones whose percentage increases. This also means that the time electrons hit the shock front (T_{in}) does not play any crucial role in controlling the relative percentages.

[53] 5. Important features are observed when both nonstationary effects along x and y are fully included. First, a large downstream heating takes place individually for each population. Second, the percentage of adiabatic electrons strongly decreases at the advantage of the "*overadiabatic*" population mainly. Third, *underadiabatic* is almost not affected.

[54] 6. In most cases, nonadiabatic populations are not issued from a certain part of the upstream distribution for a given $\widetilde{v}_{the}$ value. Only when the ramp is dominant (**R** profile), *under-* and *overadiabatic* electrons are produced in the same proportion from the core part of the upstream perpendicular distribution. This means that even a small amplitude foot (as for an **FR** profile) has a strong diffusion effect in such a way that nonadiabatic electrons can be extracted from any part of the perpendicular upstream distribution. In all cases, no dependence versus the $\widetilde{v}_{\|}$ velocity component has been noticed.

[55] **Acknowledgments.** Simulation runs have been performed on the supercomputer center IDRIS located at Orsay, France.

[56] Philippa Browning thanks the reviewer for assistance in evaluating this paper.

References

Balikhin, M. A., M. E. Gedalin, and A. Petrukovich (1993), New mechanism for electron heating in shocks, *Phys. Rev. Lett.*, *70*(9), 1259–1262.

Balikhin, M., S. Walker, T. D. de Witt, H. Alleyne, L. J. C. Woolliscroft, W. Meier-Jedrzejowicz, and W. Baumjohann (1997), Non-stationarity and low-frequency turbulence at a quasi-perpendicular shock front, *Adv. Space Res.*, *20*(4–5), 729.

Balikhin, M. A., V. Krasnosselskikh, L. J. C. Woolliscroft, and M. A. Gedalin (1998), A study of the dispersion of the electron distribution in the presence of e and b gradients: Application to electron heating

at quasi-perpendicular shocks, *J. Geophys. Res.*, *103*, 2029–2040, doi:10.1029/97JA02463.
Ball, L., and D. Galloway (1998), Electron heating by the cross-shock electric potential, *J. Geophys. Res.*, *103*, 455, doi:10.1029/98JA01185.
Ball, L., and D. B. Melrose (2001), Shock drift acceleration of electrons, *Pub. Astron. Soc. Australia*, *18*, 361–373, doi:10.1071/AS01047.
Biskamp, D., and H. Welter (1972), Numerical studies of magnetosonic collisionless shock waves, *Nucl. Fusion*, *12*, 663–666.
Cole, K. D. (1976), Effects of crossed magnetic and spatially dependent electric fields on charged particle motion, *Planet. Space. Sc.*, *24*, 515–518, doi:10.1016/0032-0633(76)90096-9.
Feldman, W. C. (1985), *Electron velocity distributions near collisionless shocks*, Collisionless shocks in Heliosphere: Reviews of current research, T. B. Tsurutani and R. G. Stone (Eds.), 195–205 pp., Geophysical Monograph Series 35, American Geophysical Union, Washington, D. C.
Feldman, W. C., R. C. Anderson, J. R. Asbridge, S. J. Bame, J. T. Gosling, and R. D. Zwickl (1982), Plasma electron signature of magnetic reconnection to the earth's bow shock: Isee-3, *J. Geophys. Res.*, *87*, 632–642.
Forslund, D. W., K. B. Quest, J. U. Brackbill, and K. Lee (1984), Collisionless dissipation in quasi-perpendicular shocks, *J. Geophys. Res.*, *89*, 2142–2150.
Galeev, A. A., V. V. Krasnoselskikh, and V. V. Lobzin (1988), Fine structure of the front of a quasiperpendicular supercritical collisionless shock wave, *Sov. J. Plasma Phys.*, *14*(10), 697–702.
Gedalin, M., M. Balikhin, and V. Krasnosselskikh (1995a), Electron heating in quasi-perpendicular shocks, *Adv. Space Res.*, *15*(8–9), 225–233.
Gedalin, M., K. G. M., M. Balikhin, V. Krasnosselskikh, and L. J. C. Woolliscroft (1995b), Demagnetization of electrons in inhomogeneous e, b: Implications for electron heating in shocks, *J. Geophys. Res.*, *100*, 19,911–19,918, doi:10.1029/95JA01399.
Gedalin, M., K. G. M., M. Balikhin, V. Krasnosselskikh, and L. J. C. Woolliscroft (1995c), Demagnetization of electrons in electromagnetic field structure, typical for quasi-perpendicular collisionless shock front, *J. Geophys. Res.*, *100*, 9481, doi:10.1029/94JA03369.
Gedalin, M., J. A. Newbury, and C. T. Russell (2000), Numerical analysis of collisionless particle motion in an observed supercritical shock front, *J. Geophys. Res.*, *105*, 105–114, doi:10.1029/1999JA900407.
Horbury, T. S., P. J. Cargill, E. A. Lucek, A. Balogh, M. W. Dunlop, T. M. Oddy, C. Carr, P. Brown, A. Szabo, and K.-H. Fornacon (2001), Cluster magnetic field observations of the bowshock: Orientation, motion and structure, *Ann. Geophysicae*, *19*, 1399–1409.
Hull, A. J., J. D. Scudder, L. A. Frank, and W. R. Paterson (1998), Electron heating and phase space signatures at strong and weak quasi-perpendicular shocks, *J. Geophys. Res.*, *103*, 2041–2054, doi:10.1029/97JA03058.
Hull, A. J., J. D. Scudder, D. E. Larson, and R. Lin (2001), Electron heating and phase space signatures at supercritical, fast mode shocks, *J. Geophys. Res.*, *106*, 15,711–15,733, doi:10.1029/2001JA900001.
Krasnoselskikh, V., M. A. Balikhin, H. S. C. Alleyne, S. I. Klimov, W. A. C. Mier-Jedrzejowicz, A. K. Pardaens, A. Petrukovich, D. J. Southwood, T. Vinogradova, and L. J. C. Woolliscroft (1991), On the nature of low-frequency turbulence in the foot of strong quasi-pependicular shocks, *Adv. Space Res.*, *11*(9), 15.
Krauss-Varban, D. (1994), Electron acceleration at nearly perpendicular collisionless shocks 3. Downstream distributions, *J. Geophys. Res.*, *99* (A2), 2537–2551.
Krauss-Varban, D., F. G. E. Pantellini, and D. Burgess (1995), Electron dynamics and whistler waves at quasi-perpendicular shocks, *Geophys. Res. Lett.*, *22*, 2091–2094, doi:10.1029/95GL01782.
Lembège, B., and J. M. Dawson (1987), Self-consistent study of a perpendicular collisonless and nonresistive shock, *Phys. Fluids*, *30*, 1767–1788.
Lembège, B., and P. Savoini (1992), Non-stationarity of a 2-D quasi-perpendicular supercritical collisonless shock by self-reformation, *Phys. Fluids*, *AA*, 3533.
Lembège, B., P. Savoini, M. Balikhin, S. Walker, and V. Krasnoselskikh (2003), Demagnetization of transmitted electrons through a quasi-perpendicular collisionless shock, *J. Geophys. Res.*, *108*(A6), 1256, doi:10.1029/2002JA009288.
Liewer, P. C., V. D. Decyk, J. M. Dawson, and B. Lembège (1991), Numerical studies of electron dynamics in oblique quasi-perpendicular collisionless shock waves, *J. Geophys. Res.*, *96*, 9455–9465.
Montgomery, M. D., J. R. Asbridge, and S. J. Bame (1970), Vela 4 plasma observations near the Earth's bow shock, *J. Geophys. Res.*, *75*, 1217.
Newbury, J. A., and C. T. Russell (1996), Observations of a very thin collisionless shock, *Geophys. Res. Lett.*, *23*, 781, doi:10.1029/96GL00700.
Newbury, J. A., C. T. Russel, and M. Gedalin (1998), The ramp widths of high mach number, quasi-perpendicular collisionless shocks, *J. Geophys. Res.*, *103*, 29,581–29,593, doi:10.1029/1998JA900024.
Northrop, T. G. (1963), *The adiabatic motion of charged particles*, Wiley-Interscience, New York.
Savoini, P., and B. Lembège (1994), Electron dynamics in two and one dimensional oblique supercritical collisionless magnetosonic shocks, *J. Geophys. Res.*, *99*, 6609–6635.
Savoini, P., B. Lembege, V. Krasnosselskhik, and Y. Kuramitsu (2005), Under and over-adiabatic electrons through a perpendicular collisionless shock: theory versus simulations, *Ann. Geophys.*, *23*, 3685–3698.
Scholer, M., I. Shinohara, and S. Matsukiyo (2003), Quasi-perpendicular shocks: Length scale of the cross-shock potential, shock reformation, and implication for shock surfing, *J. Geophys. Res.*, *108*(A1), 1014, doi:10.1029/2002JA009515.
Schwarz, S. J., M. F. Thomsen, S. J. Bame, and J. Stansberry (1988), Electron heating and the potential jump across fast mode shocks, *J. Geophys. Res.*, *93*, 12,923–12,931.
Scudder, J. D. (1995), A review of the physics of electron heating at collisionless shocks, *Adv. Space Res.*, *15*, 181–223.
Scudder, J. D., A. Mangeney, C. Lacombe, C. C. Harvey, and T. L. Aggson (1986a), The resolved layer of a collisionless, high β, supercritical, quasi-perpendicular shock wave. 2. dissipative fluid electrodynamics, *J. Geophys. Res.*, *91*, 11,053–11,073.
Scudder, J. D., A. Mangeney, C. Lacombe, C. C. Harvey, T. L. Aggson, R. R. Anderson, J. T. Gosling, G. Pashmann, and C. T. Russell (1986b), The resolved layer of a collisonless, high β, supercritical, quasi-perpendicular shock wave. 1. Rankine-Hugoniot geometry, currents, and stationarity, *J. Geophys. Res.*, *91*, 11,019–11,052.
Scudder, J. D., A. Mangeney, C. Lacombe, C. C. harvey, C. S. Wu, and R. R. Anderson (1986c), The resolved layer of a collisionless, high β, supercritical, quasi-perpendicular shock wave. 3. Vlasov electrodynamics, *J. Geophys. Res.*, *91*, 11,075–11,097.
Walker, S. N., M. A. Balikhin, H. S. C. K. Alleyne, W. Baumjohann, and M. Dunlop (1999a), Observations of a very thin shock, *Adv. Space Res.*, *24*, 47–50.
Walker, S. N., M. A. Balikhin, and M. N. Nozdrachev (1999b), Ramp nonstationarity and the generation of whistler waves upstream of a strong quasiperpendicular shock, *Geophys. Res. Lett.*, *26*, 1357–1360.
Winske, D., and K. B. Quest (1988), Magnetic field and density fluctuations at perpendicular supercritical collisionless shocks, *J. Geophys. Res.*, *93*, 9681–9693.

P. Savoini, LPP-UPMC, Ecole polytechnique, Route de Saclay, 91128 Palaiseau, France. (philippe.savoini@upmc.fr)
B. Lembege, LATMOS-UVSQ-CNRS-IPSL, Quartier des Garennes, 11 Boulevard d'Alembert, 78280 Guyancourt, France. (bertrand.lembege@latmos.ipsl.fr)